MOLECULAR IMAGING AND BIOLOGY

Mol Imaging Biol (2016) 18:99–108
DOI: 10.1007/s11307-015-0873-1

Published Online: 30 June 2015

RESEARCH ARTICLE

Comparison of Somatostatin Receptor 2-Targeting PET Tracers in the Detection of Mouse Atherosclerotic Plaques

Petteri Rinne,[1] Sanna Hellberg,[1] Max Kiugel,[1] Jenni Virta,[1] Xiang-Guo Li,[1] Meeri Käkelä,[1] Kerttuli Helariutta,[2] Pauliina Luoto,[1] Heidi Liljenbäck,[1,3] Harri Hakovirta,[4] Maria Gardberg,[5] Anu J. Airaksinen,[2] Juhani Knuuti,[1] Antti Saraste,[1,6] Anne Roivainen[1,3]

[1]*Turku PET Centre, Turku University Hospital and University of Turku, Kiinamyllynkatu 4-8FI-20520Turku, Finland*
[2]*Laboratory of Radiochemistry, Department of Chemistry, University of Helsinki, Helsinki, Finland*
[3]*Turku Center for Disease Modeling, University of Turku, Turku, Finland*
[4]*Department of Surgery, University of Turku, Turku, Finland*
[5]*Department of Pathology, Turku University Hospital and University of Turku, Turku, Finland*
[6]*Heart Center, Turku University Hospital and University of Turku, Turku, Finland*

Abstract

Purpose: Rupture-prone atherosclerotic plaques are characterized by accumulation of macrophages, which have shown to express somatostatin type 2 receptors. We aimed to investigate whether somatostatin receptor-targeting positron emission tomography (PET) tracers, [^{68}Ga]DOTANOC, [^{18}F]FDR-NOC, and [^{68}Ga]DOTATATE, can detect inflamed atherosclerotic plaques.

Procedures: Atherosclerotic IGF-II/LDLR$^{-/-}$ApoB$^{100/100}$ mice were studied *in vivo* and *ex vivo* for tracer uptake into atherosclerotic plaques. Furthermore, [^{68}Ga]DOTANOC and [^{68}Ga]DOTATATE were compared in a head-to-head setting for *in vivo* PET/X-ray computed tomography (CT) imaging characteristics.

Results: Ex vivo uptake of [^{68}Ga]DOTANOC and [^{68}Ga]DOTATATE in the aorta was higher in atherosclerotic mice compared to control C57Bl/6N mice, while the aortic uptake of [^{18}F]FDR-NOC showed no genotype difference. Unlike [^{18}F]FDR-NOC, [^{68}Ga]DOTANOC and [^{68}Ga]DOTATATE showed preferential binding to atherosclerotic plaques with plaque-to-wall ratio of 1.7±0.3 and 2.1±0.5, respectively. However, the aortic uptake and aorta-to-blood ratio of [^{68}Ga]DOTANOC were higher compared to [^{68}Ga]DOTATATE in *in vivo* PET/CT imaging.

Conclusion: Our results demonstrate superior applicability for [^{68}Ga]DOTANOC and [^{68}Ga]DOTATATE in the detection of atherosclerotic plaques compared to [^{18}F]FDR-NOC.

Key words: Somatostatin receptor, Atherosclerosis, Biodistribution, Autoradiography, Positron emission tomography

Introduction

Coronary artery disease, arising from atherosclerotic lesion formation, is one of the major causes of morbidity and mortality worldwide. The underlying disease is characterized

Petteri Rinne and Sanna Hellberg contributed equally to this work.
Electronic supplementary material The online version of this article (doi:10.1007/s11307-015-0873-1) contains supplementary material, which is available to authorized users.

Correspondence to: Anne Roivainen; *e-mail:* anne.roivainen@utu.fi

by chronic inflammation and luminal narrowing of arteries [1, 2]. The disease progression can eventually lead to plaque rupture and thrombosis manifesting as stroke or myocardial infarction. Atherosclerotic lesions that are most vulnerable to rupture are composed typically of high amounts of infiltrated macrophages and a thin fibrotic cap lining the inner surface of the plaque [3, 4]. Active inflammation is detectable at all stages of the disease and an emerging target for the imaging and treatment of the disease. Noninvasive imaging methods targeting the inflammatory processes offer a promising tool to identify patients at high risk of plaque rupture [5, 6].

Molecular imaging with 2-deoxy-2-[^{18}F]fluoro-*D*-glucose ([^{18}F]FDG) positron emission tomography (PET)/X-ray computed tomography (CT) is a well-established method to noninvasively detect and quantify plaque inflammation in large peripheral arteries [7]. Accumulation of [^{18}F]FDG into atherosclerotic arteries has shown to correlate with histological features of inflammation and particularly with the plaque macrophage count [8, 9]. Expanding this into clinical significance that can help to guide therapy, it has also been demonstrated that arterial [^{18}F]FDG uptake is sensitive for anti-atherosclerotic treatment and it can predict plaque rupture and thrombotic complications [10–12]. A major limitation of [^{18}F]FDG-PET/CT imaging is, however, the nonspecific nature of [^{18}F]FDG uptake as its accumulation into atherosclerotic lesions can be driven by factors other than activated macrophages [13]. Additionally, limiting the feasibility of [^{18}F]FDG-PET/CT imaging of diseased coronary arteries, [^{18}F]FDG physiologically accumulates into the myocardium and thus obscures the identification of coronary pathologies [6].

Offering an alternative to [^{18}F]FDG, recent studies have implicated somatostatin receptors as a viable target for molecular imaging of plaque inflammation. Murine and human macrophages express especially somatostatin type 2 receptors (SSTR-2), which can be detected with the PET tracer ^{68}Ga-[1,4,7,10-tetraazacyclododecane-*N,N′,N″,N‴*-tetraacetic acid]-d-Phe^{1}-Tyr^{3}-octreotate ([^{68}Ga]DOTATATE) [14, 15]. The uptake of [^{68}Ga]DOTATATE to coronary arteries is significantly associated with the degree of plaque calcification and traditional cardiovascular risk factors such as age, male sex, and hypertension [14, 16]. SSTR-targeting PET tracers were originally developed to aid the diagnosis of neuroendocrine tumors and this concept has been adopted in several imaging units where other similar tracers, besides [^{68}Ga]DOTATATE, are routinely used. The aim of the present study was to investigate the usability of two other SSTR-targeting PET tracers, which readily bind to the SSTR-2 subtype, in the detection of inflamed atherosclerotic plaques. We aimed to study [^{68}Ga]DOTA-Nal^{3}-octreotide ([^{68}Ga]DOTANOC) and a novel glycosylated peptide tracer, 5-deoxy-5-[^{18}F]fluororibose-NOC ([^{18}F]FDR-NOC), in terms of their uptake into mouse atherosclerotic plaques, and compare their characteristics with [^{68}Ga]DOTATATE. [^{68}Ga]DOTANOC has been successfully used for the imaging of various tumors and has high affinity for SSTR-2 [17, 18]. [^{18}F]FDR-NOC also targets SSTR-2 subtype and was recently reported to display a distinct kinetic profile but similar target binding properties to [^{68}Ga]DOTANOC [19].

Materials and Methods

Animals and General Study Design

All animal experiments were approved by the national Animal Experiment Board in Finland (ELLA) and the Regional State Administrative Agency for Southern Finland (ESAVI) and conducted in accordance with the European Union Directive. Male and female IGF-II/LDLR$^{-/-}$ApoB$^{100/100}$ mice were studied as an experimental model of atherosclerosis [20, 21]. IGF-II/LDLR$^{-/-}$ApoB$^{100/100}$ mice were fed an atherogenic diet (0.2 % total cholesterol, TD 88137, Harlan Teklad, Harlan Laboratories, Madison, WI, USA) for 4–5 months starting at the age of 2–4 months, and used for *in vivo* and *ex vivo* experiments at the age of 6–9 months. C57Bl/6 N mice, maintained on regular chow diet, were studied as non-atherosclerotic controls. Numbers of mice studied are given in Table 1.

First, the presence of SSTR-2 was studied in mouse and human atherosclerotic arteries. The *in vivo* stability and specificity of the new SSTR-2 targeting tracer [^{18}F]FDR-NOC, was studied by HPLC of plasma and urine samples, and by *in vivo* blocking study (described in the supplementary data). [^{18}F]FDR-NOC, [^{68}Ga]DOTANOC and [^{68}Ga]DOTATATE were then compared by conducting *in vivo* imaging, *ex vivo* biodistribution, and aortic autoradiography. The uptakes of [^{18}F]FDR-NOC and [^{68}Ga]DOTANOC were compared with the levels of pro-inflammatory cytokines and metabolic markers in the plasma. Finally, [^{68}Ga]DOTANOC and [^{68}Ga]DOTATATE were compared in a head-to-head setting *in vivo*.

SSTR-2 Immunohistochemistry

SSTR-2 immunohistochemistry was performed on the 8-μm cryosections adjacent to the 20-μm slides used for autoradiography analysis and on 8-μm cryosections from a human carotid endarterectomy sample, which was obtained from a patient with a recent ischemic stroke. The patient study was conducted according to the declaration of Helsinki, and the study protocol was approved by the ethics committee of Hospital District of Southwest Finland.

The frozen slides were fixed in cold acetone for 5 min, and stained with an SSTR-2 monoclonal antibody (clone UMB-1) from Abcam (Cambridge, UK) using a LabVision autostainer with BrightVision detection kit (Immunologic, Duiven, the Netherlands). The SSTR-2 antibody was used at 1:100 dilution with 60 min incubation at room temperature. This antibody has previously been thoroughly characterized [22]. In negative controls the primary antibody was omitted from the protocol.

Preparation of Radiotracers

The radiosynthesis of [^{68}Ga]DOTANOC was performed with a fully automated synthesis device (Modular Lab, Eckert & Ziegler Eurotope GmbH, Berlin, Germany) [23]. Radiochemical purity and specific

Table 1. Characteristics of mice

	Control		Atherosclerotic	
Tracer	*n* (m/f)	Weight (g)	*n* (m/f)	Weight (g)
[^{68}Ga]DOTANOC	11 (7/4)	26.5±5.6	16 (8/8)	32.1±7.1
[^{18}F]FDR-NOC	6 (6/0)	40.1±4.2	9 (8/1)	34.2±8.4
[^{68}Ga]DOTATATE	4 (0/4)	23.3±1.9	6 (0/6)[a]	24.2±2.6

Values are mean±SD
n number of mice, *m/f* males/females
[a]*In vivo* imaging with [^{68}Ga]DOTANOC prior to imaging with [^{68}Ga]DOTATATE for head-to-head comparison between these tracers

radioactivity (mean) of [^{68}Ga]DOTANOC was>99 % and 30.8 GBq/μmol, respectively. The tracer [^{18}F]FDR-NOC was prepared according to known protocols [24, 25]. Briefly, 5-deoxy-5-[^{18}F]-fluororibose as a prosthetic group was conjugated to the somatostatin analogue NOC peptide (0.3 mM, ABX GmbH, Radeberg, Germany) in anilinium buffer (0.3 M, pH 4.6) for 10 min at room temperature. The reaction mixture was subjected to high-performance liquid chromatography (HPLC) purification with a Jupiter Proteo C18 column (250×10 mm, Phenomenex Inc, Torrance, CA, USA). [^{18}F]FDR-NOC was formulated in phosphate-buffered saline (PBS) with a sterile filtration (0.22 μm) for injection. The radiochemical purity was >99 % and specific radioactivity 39.6–40.5 GBq/μmol at the end of synthesis. The total preparation time was 146–161 min starting from end of bombardment. For the Ga-68 labelling of DOTATATE, Ga-68 was obtained from a ^{68}Ge/^{68}Ga generator (Eckert & Ziegler, CA, USA) by elution with 0.1 M HCl and the radioactive elution peak was collected. Ga-68 eluate (500 μl) was mixed with HEPES (120 mg) to give a pH of approximately 5 and thereafter DOTATATE (1 mM, Peptide Specialty Laboratories GmbH, Heidelberg, Germany) was added to the mixture. The reaction mixture was then heated at 100 °C for 10 min. Radiochemical purity of [^{68}Ga]DOTATATE was determined by reversed phase HPLC with Jupiter C18 column (4.6×150 mm, Phenomenex, Inc). The radiochemical purity was >96 % and specific radioactivity 30.3–33.0 GBq/μmol at the end of synthesis.

Ex Vivo Biodistribution and Autoradiography

Mice were fasted with *ad libitum* access to water for 4 h before tracer injection. The mice were anesthetized with isoflurane and injected with [^{68}Ga]DOTANOC (7.4±1.5 MBq), [^{18}F]FDR-NOC (10.2±0.9 MBq), or [^{68}Ga]DOTATATE (6.9±0.2 MBq) *via* a tail vein catheter. After 60 min, the mice were euthanized and the aorta from the sinotubular junction to the level of the diaphragm was dissected and rinsed with saline to remove blood. Radioactivity concentration in excised organs was measured with a gamma counter (Triathler 3″, Hidex, Turku, Finland or 1480 Wizard 3″ Gamma Counter; Perkin Elmer/Wallac, Turku, Finland) to determine the *ex vivo* biodistribution in atherosclerotic and control mice. Measured radioactivity was corrected for decay, weight of the organ and animal, and background radioactivity, and it was expressed as standardized uptake value (SUV). After gamma counting, the aorta was frozen, cut into sequential longitudinal 20- and 8-μm cryosections with a cryomicrotome at −15 °C and thaw-mounted onto microscope slides for autoradiography (ARG) studies.

ARG analysis was performed to determine the distribution in aortic tissue. Briefly, longitudinal 20-μm cryosections of the aorta were apposed to an imaging plate (Fuji Imaging Plate BAS-TR2025, Fuji Photo Film Co., Ltd., Tokyo, Japan). After an exposure time of 4 h, the imaging plates were scanned with Fuji Analyzer BAS-5000 (internal resolution of 25 μm) or Fuji FLA-5100 (internal resolution 10 μm). The 20-μm sections were stained with hematoxylin and eosin (H&E), and 6 to 8 sections from each mouse were then examined for morphology under a light microscope. After a careful co-registration of the autoradiographs and H&E images, Ga-68 and F-18 radioactivity was measured from non-calcified atherosclerotic plaques (excluding media), normal arterial walls (no lesion formation) and adventitia (including perivascular adipose tissue), and expressed as photostimulated luminescence intensity per unit area (PSL per square millimeter) using Tina 2.1 software (Raytest Isotopemessgeräte, GmbH, Straubenhardt, Germany). The radioactivity uptake was also evaluated as plaque-to-wall and plaque-to-adventitia ratios. Cryosections (8 μm) adjacent to ARG-analyzed sections were immunohistochemically stained with a macrophage specific anti-mouse antibody (Mac-3, clone m3/84, BD Biosciences Pharmingen, Franklin Lakes, NJ, USA) to detect inflamed atherosclerotic plaques as previously described [26, 27].

In Vivo PET/CT Imaging

A subset (n=2–4) of mice studied with [^{68}Ga]DOTANOC or [^{18}F]FDR-NOC and all the mice studied with [^{68}Ga]DOTATATE were *in vivo* imaged with an Inveon Multimodality PET/CT scanner (Siemens Medical Solutions, Knoxville, TN, USA) before *ex vivo* biodistribution and autoradiography studies. Dynamic acquisition, consisting of 11 time frames (2×30 s, 4×60 s and 5×300 s), was started immediately after intravenous tracer injection. Thereafter, CT angiography was performed using vascular contrast agent (eXIA160XL, Binitio Biomedical Inc, Ottawa, ON, Canada). Quantitative PET analysis was performed by defining regions of interest (ROIs) for the aortic arch, heart, and inferior vena cava (blood pool) using Carimas software (Carimas 2.8; Turku PET Centre, Turku, Finland). The CT template was used as anatomical reference. The radioactivity concentrations were corrected for injected radioactivity dose and decay, and the results were presented as standardized uptake value (SUV) and time-radioactivity curves (TACs).

Cytokine and Metabolic Hormone Measurements in Mouse Plasma

It was further investigated whether the uptake of [^{68}Ga]DOTANOC or [^{18}F]FDR-NOC is correlated with pro-inflammatory cytokine and metabolic hormone levels. Plasma levels of interleukin 6 (IL-6), monocyte chemotactic protein 1 (MCP-1), RANTES (regulated on activation, normal T cell expressed and secreted), C-peptide, insulin, and leptin were measured using a Luminex assay according to the manufacturer's instructions (MILLIPLEX, MMHMAG-44K and MCYTOMAG-70K, Magnetic Bead Panel, Merck Millipore, MA, USA). The minimum detectable concentrations (picogram per milliliter) for the analytes were 1.1 (IL-6), 6.7 (MCP-1), 2.7 (RANTES), 20 (C-peptide), 14 (insulin), and 19 (leptin).

Head-to-Head Comparison of [^{68}Ga]DOTANOC and [^{68}Ga]DOTATATE

The *in vivo* imaging performance of [^{68}Ga]DOTANOC and [^{68}Ga]DOTATATE was compared by performing PET/CT with both tracers for the same atherosclerotic mice. The mice were injected with [^{68}Ga]DOTANOC (6.1±0.9 MBq) and *in vivo* imaged with the Inveon Multimodality PET/CT scanner using the same acquisition protocol as described above. Six to seven days later, [^{68}Ga]DOTATATE imaging was performed for the same mice followed by *ex vivo* biodistribution and autoradiography as described above.

Statistical Analysis

All data are expressed as mean±SD. Comparisons were made by Student's *t* test or one-way analysis of variance (ANOVA) followed by Bonferroni *post hoc* tests. Biodistribution data was corrected for multiple comparisons using the Holm-Sidak method. In ARG analysis, one sample *t* test was used to test deviation of plaque-to-wall and plaque-to-adventitia ratios from a hypothetical value of 1.0. Pearson correlation coefficients were calculated for associations between *ex vivo* radioactivities and plasma cytokines. A two-tailed *P* value of less than 0.05 was considered statistically significant.

Results

Mouse and Human Atherosclerotic Plaques Show Positive Staining for SSTR-2

To verify the expression of the tracer target in atherosclerotic plaques, aortic longitudinal sections from IGF-II/LDLR$^{-/-}$ApoB$^{100/100}$ mice were immunostained for SSTR-2. Positive SSTR-2 staining was observed on the luminal side of plaques (Fig. 1a), while arterial walls showed only weak and occasional SSTR-2 expression. Positive SSTR-2 staining was also detectable in human endarterectomy sample of atherosclerotic carotid artery (Fig. 1b).

Ex Vivo Biodistribution of [^{68}Ga]DOTANOC, [^{18}F]FDR-NOC, and [^{68}Ga]DOTATATE Radioactivities in Control and Atherosclerotic IGF-II/LDLR$^{-/-}$ApoB$^{100/100}$ Mice

Biodistribution of SSTR-targeting tracers, [^{68}Ga]DOTANOC,[^{18}F]FDR-NOC, and [^{68}Ga]DOTATATE, were studied in Western-diet fed IGF-II/LDLR$^{-/-}$ApoB$^{100/100}$ mice. This mouse model has previously been shown to develop major plaque burden not only in the aortic arch but also in the descending parts of the aorta and to display elevated uptake of [^{18}F]FDG in plaque areas, depicting augmented metabolic activity [20, 21]. *Ex vivo* biodistribution of [^{68}Ga]DOTANOC revealed significantly increased uptake of the tracer in the whole aorta of atherosclerotic mice (SUV values 1.02±0.36) compared to control mice (0.43±0.18) at 60-min post-injection (Fig. 2a). However, atherosclerotic mice showed also elevated [^{68}Ga]DOTANOC uptake in several other tissues including the blood and heart, resulting in similar aorta-to-blood (1.2±0.3 *vs.* 1.3±0.3 in control, P=0.14) and aorta-to-heart (5.8±1.2 *vs.* 5.2±1.8 in control, P=0.38) ratios between the genotypes.

In contrast to [^{68}Ga]DOTANOC, the uptake [^{18}F]FDR-NOC in the aorta of atherosclerotic mice was comparable to that of control mice (Fig. 2b). [^{18}F]FDR-NOC showed accumulation particularly to the liver and kidney. However, there was no clear-cut difference in the distribution profile of [^{18}F]FDR-NOC between the genotypes. Aorta-to-blood ratio was 1.0±0.2 in atherosclerotic and 1.2±0.6 in control mice (P=0.38). Furthermore, no difference was noted in the aorta-to-heart ratio (4.9±1.0 *vs.* 5.6±2.5 in control, P=0.48).

Similarly to [^{68}Ga]DOTANOC, the uptake of [^{68}Ga]DOTATATE in the aorta was higher in atherosclerotic mice compared to control mice (Fig. 2c). However, [^{68}Ga]DOTATATE showed also increased uptake in other tissues of atherosclerotic mice, including the blood, which resulted in low aorta-to-blood ratio (0.5±0.1 *vs.* 0.6±0.1 in control, P=0.11).

[^{68}Ga]DOTANOC and [^{68}Ga]DOTATATE Preferentially Bind to Atherosclerotic Plaques

Autoradiographs of aortic longitudinal cross-sections were superimposed on corresponding H&E-stained images and analyzed for relative tracer uptake in non-calcified atherosclerotic plaques, non-atherosclerotic vessel wall, and adventitia. ARG analysis revealed higher uptake of [^{68}Ga]DOTANOC in atherosclerotic plaques than in normal vessel wall or adventitia (Fig. 3a, c). Plaque-to-wall ratio was 1.7±0.3 (P<0.0001) and plaque-to-adventitia ratio 1.7±0.3 (P<0.0001). Immunostaining with Mac-3 antibody confirmed that [^{68}Ga]DOTANOC radioactivity was concentrated in macrophage-rich regions (Fig. 3b). Accumulation of [^{18}F]FDR-NOC in

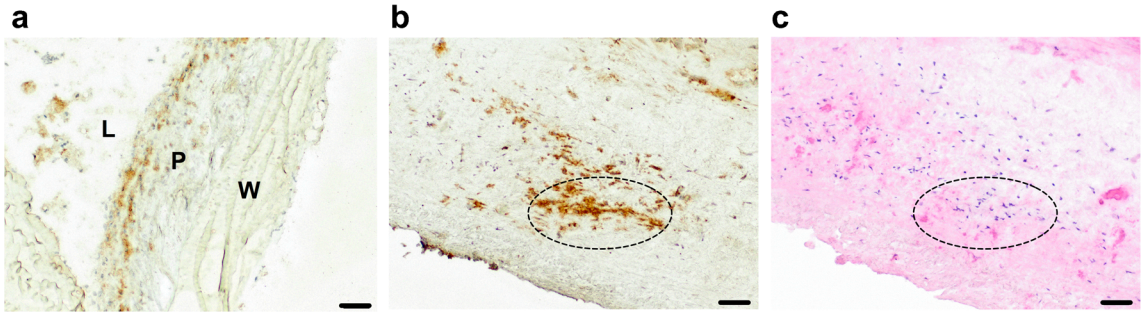

Fig. 1 Expression of somatostatin receptor subtype-2 (SSTR-2) in mouse and human atherosclerotic plaques. **a** Longitudinal aortic section of an IGF-II/LDLR$^{-/-}$ApoB$^{100/100}$ mouse showing positive staining for SSTR-2 in atherosclerotic plaque but not in vessel wall. *Brown staining* indicates antibody recognition. Sections were counterstained with hematoxylin. *L*, lumen; *P*, plaque; *W*, wall. **b** Endarterectomy section from a human atherosclerotic carotid artery stained with the SSTR-2-specific antibody. **c** Adjacent section from the same sample stained with H&E. *Dotted circles* illustrate the colocalization of SSTR-2 staining with an area of high nuclear density. *Scale bar* is 50 μm in each figure.

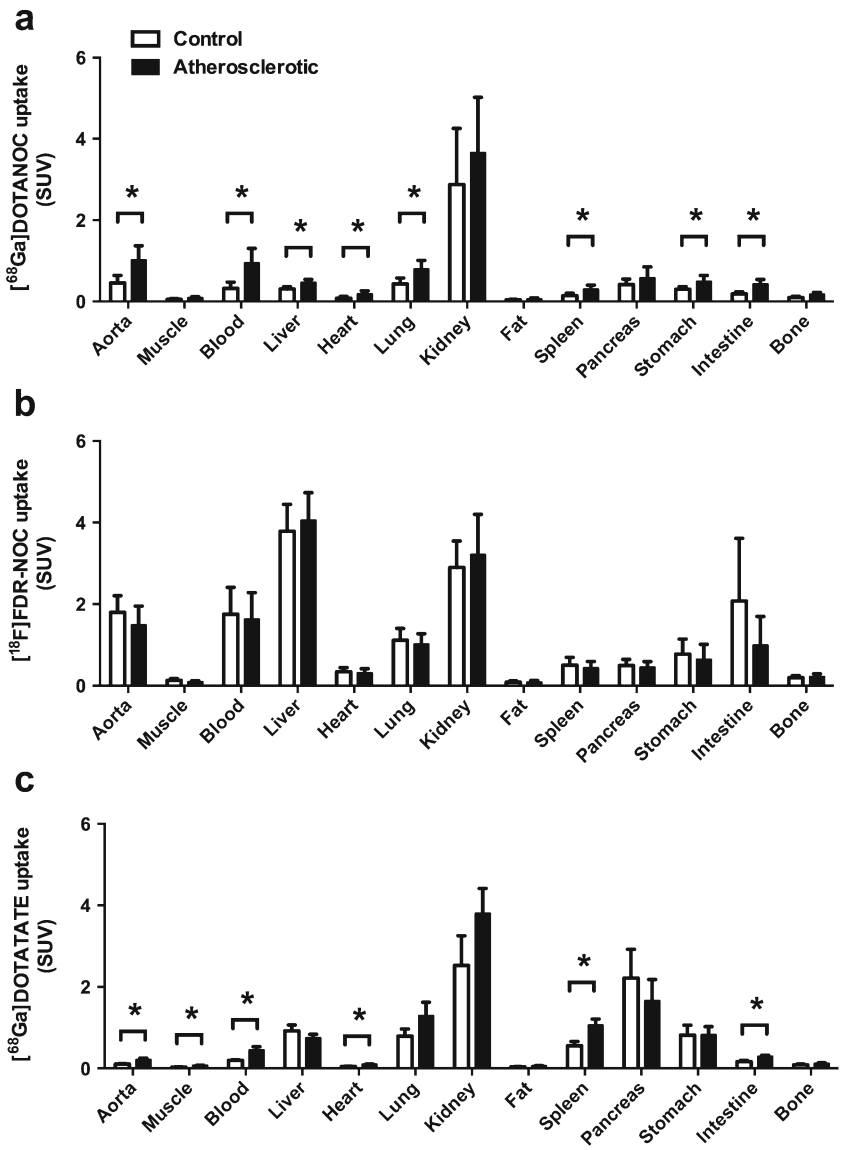

Fig. 2 Biodistribution of [^{68}Ga]DOTANOC, [^{18}F]FDR-NOC and [^{68}Ga]DOTATATE in control and atherosclerotic mice. **a** Tissue uptake characteristics of [^{68}Ga]DOTANOC at 60 min after injection. Results are expressed as standardized uptake values (SUV). *$P<0.05$ *versus* control mice after correction for multiple comparisons. **b** Biodistribution of [^{18}F]FDR-NOC at 60 min after injection. **c** Biodistribution of [^{68}Ga]DOTATATE at 60 min after injection. Values are mean±SD.

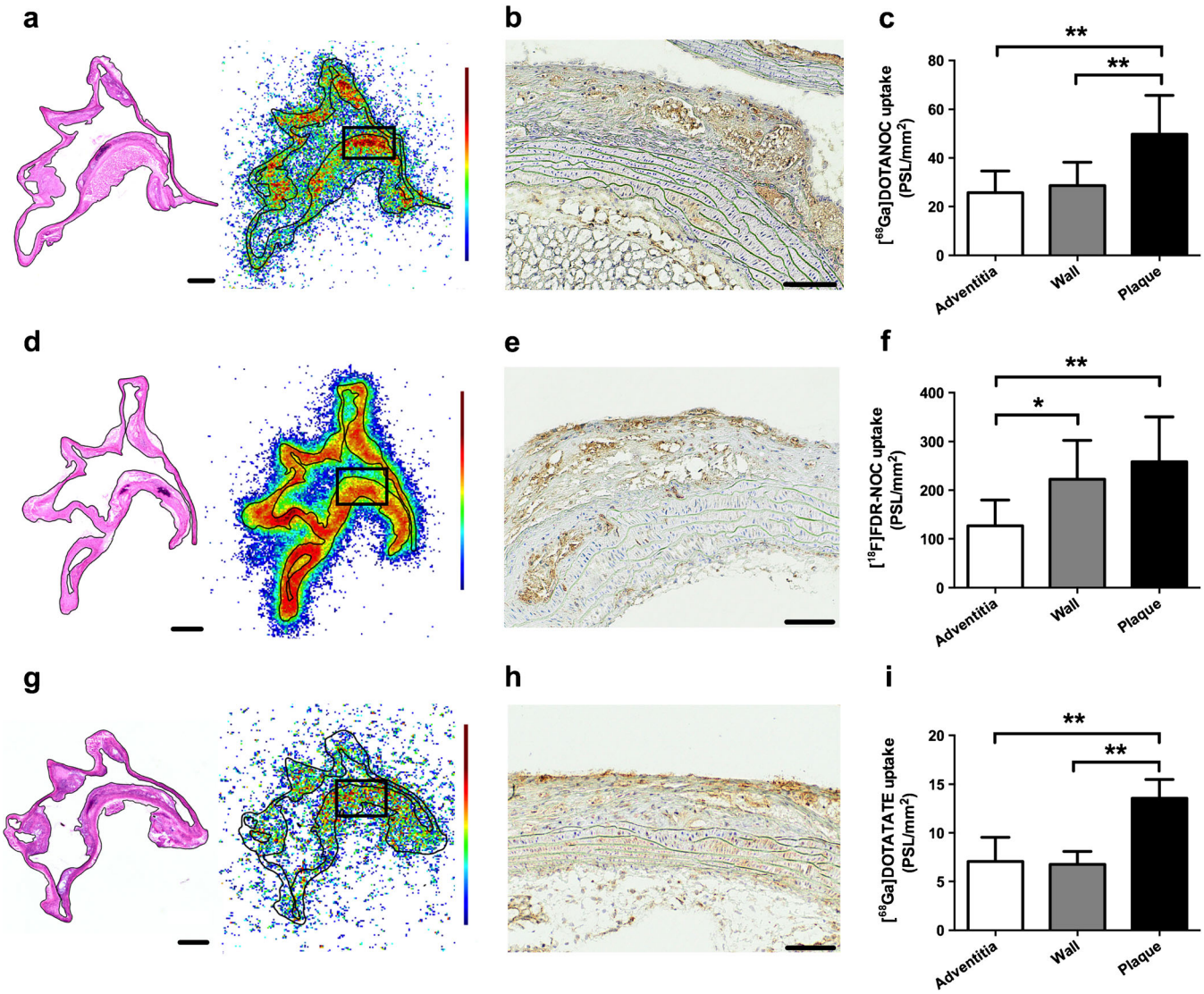

Fig. 3 Autoradiography of [^{68}Ga]DOTANOC, [^{18}F]FDR-NOC and [^{68}Ga]DOTATATE in mouse atherosclerotic plaques. Representative aortic longitudinal sections stained with H&E and their corresponding autoradiographs for **a** [^{68}Ga]DOTANOC, **b** [^{18}F]FDR-NOC, and **g** [^{68}Ga]DOTATATE. H&E-stained sections show the aortic arch and major arteries branching off from the aorta. *Scale bar* is 500 μm. **b, e**, and **h**: Adjacent sections stained with the Mac-3 antibody showing the presence of infiltrated macrophages in atherosclerotic plaques of IGF-II/LDLR$^{-/-}$ApoB$^{100/100}$ mice. *Scale bar*, 100 μm. **c**, **f**, and **i**: Quantification of the digital autoradiographs showing the distribution of [^{68}Ga]DOTANOC, [^{18}F]FDR-NOC, and [^{68}Ga]DOTATATE radioactivity in adventitia, non-atherosclerotic vessel walls, and atherosclerotic plaques. Results (mean±SD) are expressed as photostimulated luminescence per unit area (PSL per square millimeter).

atherosclerotic plagues was only marginally higher compared to uptake in non-atherosclerotic vessel wall (plaque-to-wall ratio 1.2±0.2, P=0.04) (Fig. 3d, f). However, [^{18}F]FDR-NOC uptake was lower on the adventitial side of aorta compared to vessel wall, thus giving a higher plaque-to-adventitia ratio (2.1±0.4, P<0.0001). [^{68}Ga]DOTATATE accumulated markedly more in atherosclerotic plaques compared to non-atherosclerotic arterial walls or adventitial tissue (Fig. 3g, i), but it was of note that the normalized radioactivity values (PSL/mm^2) of plaques as well as of arterial walls and adventitia were much lower compared to those of [^{68}Ga]DOTANOC. Plaque-to-wall ratio of [^{68}Ga]DOTATATE uptake was 2.1±0.5 in atherosclerotic mice.

In Vivo PET/CT Imaging

A subset of atherosclerotic and control mice underwent a 30-min dynamic PET/CT scan after the injection of [^{68}Ga]DOTANOC, [^{18}F]FDR-NOC, or [^{68}Ga]DOTATATE (Fig. 4). At 30-min post-injection, the *in vivo* uptake of [^{68}Ga]DOTANOC in the aortic arch was 1.0±0.1 in atherosclerotic mice and 0.6±0.1 in control mice (Fig. 4b).

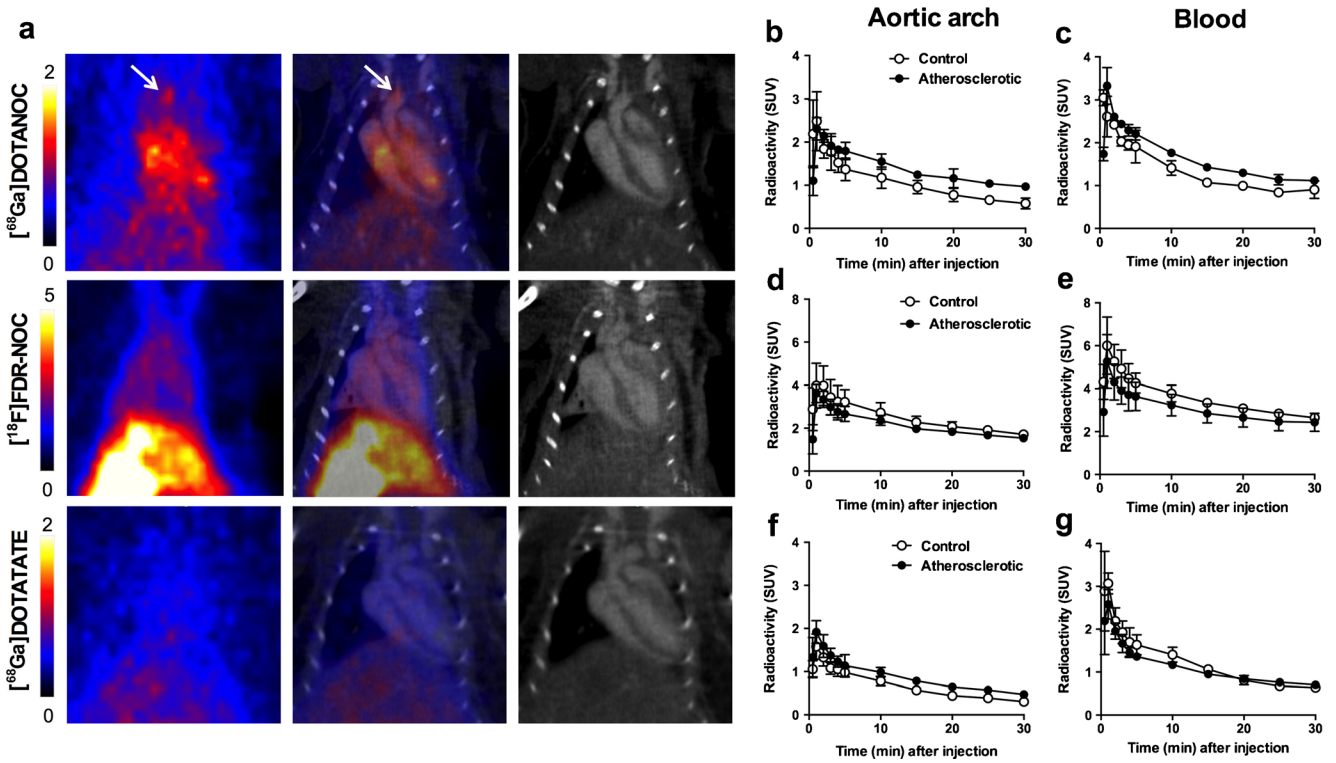

Fig. 4 *In vivo* PET/CT imaging. **a** Representative *in vivo* PET (*left*), CT angiography (*right*), and fused PET/CT (*middle*) images showing focal (*white arrows*) uptake of [^{68}Ga]DOTANOC, [^{18}F]FDR-NOC and [^{68}Ga]DOTATATE in the brachiocephalic artery of an atherosclerotic IGF-II/LDLR$^{-/-}$ApoB$^{100/100}$ mouse. Images represent the last 5-min frame of 30-min dynamic imaging. Time-activity curves of aortic arc (**b**, **d**, and **f**) and blood (**c**, **e**, and **g**) in atherosclerotic and control mice after tracer injection. Values are mean±SD.

In line with the *ex vivo* biodistribution results, [^{68}Ga]DOTANOC time-radioactivity curves revealed increased tracer uptake also in the blood of atherosclerotic mice (Fig. 4c). In terms of [^{18}F]FDR-NOC uptake, atherosclerotic mice did not differ from control mice. The aortic as well as blood [^{18}F]FDR-NOC radioactivity curves of atherosclerotic mice closely paralleled those of control mice (Fig. 4d, e). The uptake of [^{68}Ga]DOTATATE was higher in the aortic arch of atherosclerotic mice compared to control mice (Fig. 4f), while no difference between the genotypes was observed in the blood uptake values (Fig. 4g).

Correlation of [^{68}Ga]DOTANOC and [^{18}F]FDR-NOC Uptake to Plasma Cytokine and Metabolic Hormone Markers

Plaque-to-wall ratios of tracer uptake were plotted against plasma levels of IL-6, MCP-1, RANTES, C-peptide, insulin, and leptin (Fig. 5). Plaque-to-wall ratio of [^{68}Ga]DOTANOC was found to directly associate with plasma IL-6 levels (Fig. 5a). There was also a tendency for positive correlation to MCP-1 (Fig. 5b). In addition to cytokines, [^{68}Ga]DOTANOC uptake positively correlated with insulin and leptin levels (Fig. 5e, f). No statistically significant correlations between [^{18}F]FDR-NOC and plasma cytokines or metabolic hormones were found (data not shown).

Head-to-Head Comparison of [^{68}Ga]DOTANOC and [^{68}Ga] DOTATATE In Vivo

Since [^{68}Ga]DOTATATE has shown promising characteristics for atherosclerosis imaging in previous studies, [^{68}Ga]DOTATATE and [^{68}Ga]DOTANOC were compared in terms of their uptake into atherosclerotic arteries in a head-to-head setting *in vivo*. The results revealed that the uptake of [^{68}Ga]DOTANOC was higher particularly in the aortic arch (Fig. 6a). Importantly, [^{68}Ga]DOTANOC showed better aorta-to-blood ratio of tracer uptake at the end of the imaging (0.83±0.07 *vs.* 0.67±0.04 for [^{68}Ga]DOTATATE, $P<0.01$) (Fig. 6c).

Discussion

In the present study, we compared the SSTR-2-targeting radiotracers, [^{68}Ga]DOTANOC, [^{18}F]FDR-NOC and [^{68}Ga]DOTATATE, for their ability to detect macrophage-rich atherosclerotic plaques. We found that the uptake of [^{68}Ga]DOTANOC as well as of [^{68}Ga]DOTATATE was higher in plaques than in non-atherosclerotic arterial walls, while [^{18}F]FDR-NOC showed no preferential binding to atherosclerotic lesions. Of note, [^{68}Ga]DOTANOC showed better characteristic for *in vivo* PET imaging compared to [^{68}Ga]DOTATATE. These findings support the potential use of [^{68}Ga]DOTANOC for atherosclerosis imaging.

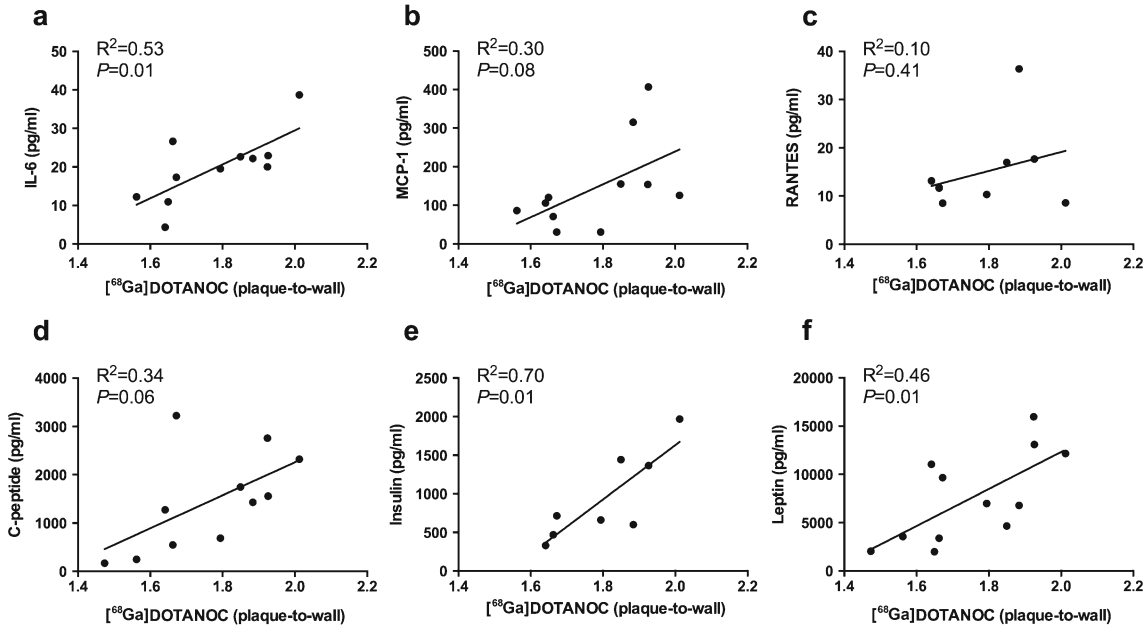

Fig. 5 Relationship between tracer uptake and plasma cytokine levels. Correlations between plaque-to-wall ratio of [^{68}Ga]DOTANOC uptake and plasma levels of **a** IL-6, **b** MCP-1, **c** RANTES, **d** C-peptide, **e** insulin, and **f** leptin. Squared Pearson correlation coefficients and *P* values are presented in the graphs.

Somatostatin is a circulating regulatory peptide that exerts its biological actions through a family of G-protein-coupled receptors [28]. The receptor family comprises five subtypes (SSTR-1 to SSTR-5), which are physiologically expressed in most organs. The expression of these receptors is upregulated in several diseases states, including neuroendocrine tumors, in which SSTR-targeting has been successfully used for imaging-based diagnosis and radionuclide therapy. Somatostatin receptors, particularly subtypes 1 and 2, are also overexpressed in activated macrophages and injured endothelium where they might have a regulatory role in modulating inflammation and angiogenesis [29, 30]. These findings have opened a new avenue of investigation in molecular imaging of atherosclerosis. [^{68}Ga]DOTATATE, which specifically binds to SSTR-2, has been previously demonstrated to be taken up by calcified arteries [14, 16]. Furthermore, SSTR-targeted radionuclide therapy was recently shown to favorably modify atherosclerotic plaque activity as evidenced by reduced [^{68}Ga]DOTATATE uptake in atherosclerotic plaques after the therapy [31]. These preliminary studies were conducted in a retrospective fashion in oncology patients and further prospective studies are warranted to explore the applicability of SSTR-imaging for detection of arterial inflammation in patients with carotid or coronary atherosclerosis.

Using SSTR-2 immunohistochemistry, we were able to confirm that the new mouse model of atherosclerosis (IGF-II/LDLR$^{-/-}$ApoB$^{100/100}$) had also significant expression of SSTR-2 in the aorta, localizing in plaque regions with no or very low expression in arterial walls. Positive staining was also noticeable in human carotid plaque sample. This confirmed the presence of the target and gave the required prerequisite to investigate whether SSTR-2 expression can be detected with the PET tracers [^{68}Ga]DOTANOC,

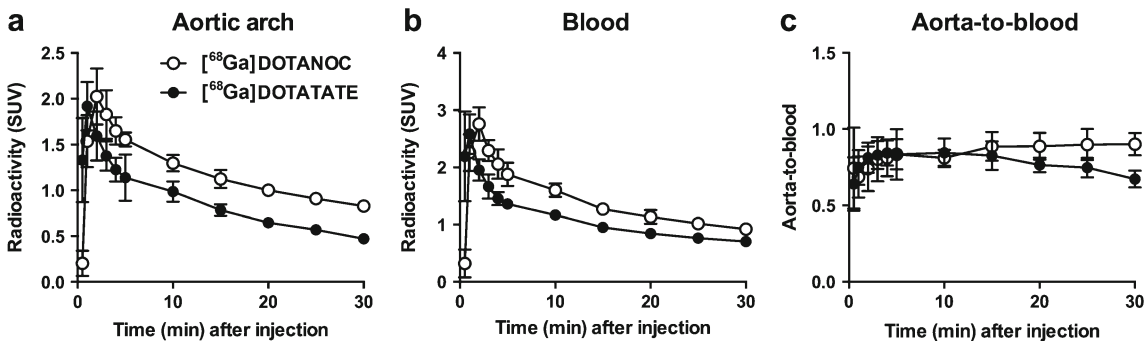

Fig. 6 Head-to-head comparison of *in vivo* imaging between [^{68}Ga]DOTANOC and [^{68}Ga]DOTATATE. Time-radioactivity curves of **a** aortic arch, **b** blood, and **c** aorta-to-blood ratio in atherosclerotic mice injected with either [^{68}Ga]DOTANOC or [^{68}Ga]DOTATATE. Values are mean±SD.

[^{18}F]FDR-NOC, and [^{68}Ga]DOTATATE. Analysis of *ex vivo* radioactivities in excised tissues revealed that [^{68}Ga]DOTANOC and [^{68}Ga]DOTATATE but not [^{18}F]FDR-NOC had accumulated more in the aorta of atherosclerotic IGF-II/LDLR$^{-/-}$ApoB$^{100/100}$ mice compared to healthy control mice. Despite the augmented uptake in the aorta, the superiority of [^{68}Ga]DOTANOC and [^{68}Ga]DOTATATE over [^{18}F]FDR-NOC was limited when assessing target-to-background ratios. The uptake of [^{68}Ga]DOTANOC and [^{68}Ga]DOTATATE was higher in several other tissues of atherosclerotic mice. Consequently, the resolution of these tracers to distinguish atherosclerotic mice from control mice was poor in our experimental setting if the judgment is based on aorta-to-blood or aorta-to-heart ratio. We are lacking a clear explanation for the distinctive pattern of increased [^{68}Ga]DOTANOC and [^{68}Ga]DOTATATE accumulation in most of the measured tissues. There might be a metabolic defect in IGF-II/LDLR$^{-/-}$ApoB$^{100/100}$ mice that retards the degradation of the tracer and/or urinary excretion, thus resulting in a high background signal in these mice. However, in line with other studies, the uptake of [^{68}Ga]DOTANOC and [^{68}Ga]DOTATATE in the heart was relatively low, which further supports the potential of SSTR-2-targeted PET imaging in patients with coronary atherosclerosis.

Corroborating the biodistribution findings, *in vivo* PET/CT imaging after [^{68}Ga]DOTANOC or [^{68}Ga]DOTATATE injection showed consistently increased tracer uptake in the aortic arch and blood. Due to the inclusion of blood pool to the ROIs drawn over the aortic arch, the uptake of the Ga-68-labelled tracers in the aorta was largely attributable to blood radioactivity and was not thus a true representative of augmented tracer uptake in atherosclerotic regions. Nevertheless, focally increased [^{68}Ga]DOTANOC uptake could be observed in the aortic arch and its major branching arteries as hot spots in the *in vivo* PET images. Aside from the observations with [^{68}Ga]DOTANOC and [^{68}Ga]DOTATATE, [^{18}F]FDR-NOC was again ineffective in revealing any genotype differences in the tracer uptake. Although the analysis of biodistribution and *in vivo* PET imaging data was biased by the generalized increase in tracer uptake across multiple tissues, further dissection of [^{68}Ga]DOTANOC and [^{68}Ga]DOTATATE uptake in atherosclerotic arteries by autoradiography analysis supported the notion that these particular tracers pose better characteristics in terms of applicability for atherosclerosis imaging. As expected from the basis of SSTR-2 immunostained arteries, [^{68}Ga]DOTANOC accumulated considerably more in atherosclerotic plaques than in normal vessel walls. The plaque-to-wall ratio of [^{68}Ga]DOTANOC averaged 1.7, which is very close to the corresponding ratio (~1.8) observed for [^{68}Ga]DOTATATE in ApoE knock-out mice [15]. The plaque-to-wall ratio for [^{68}Ga]DOTATATE averaged slightly higher (~2.1) in IGF-II/LDLR$^{-/-}$ApoB$^{100/100}$ mice used in this study, mainly due to a very low uptake in non-atherosclerotic arterial walls. In fact, *ex vivo* biodistribution and ARG analysis results as well as results from *in vivo* PET/CT imaging showed consistently lower radioactivity values in the aorta for [^{68}Ga]DOTATATE compared to [^{68}Ga]DOTANOC, which could favor the use of the latter tracer for further studies. It remains an open question why [^{18}F]FDR-NOC did not show preferential binding to atherosclerotic arteries with any of the employed methods. Based on the results showing good *in vivo* stability and specificity for [^{18}F]FDR-NOC, and considering that [^{68}Ga]DOTANOC and [^{18}F]FDR-NOC share the same SSTR-2-binding domain NaI^{3}-octreotide (NOC) [18], it was expected that the glycosylated peptide derivative [^{18}F]FDR-NOC would not show inferior characteristics in comparison with [^{68}Ga]DOTANOC. A previous study, employing a rat glioma model, demonstrated that [^{18}F]FDR-NOC, owing to its glycosylated nature, readily accumulated not only in explanted tumors but also in non-target tissues [19]. This could partly explain the present finding that the pharmacokinetics of [^{18}F]FDR-NOC was also unfavorable for the detection of atherosclerotic arteries in mice.

We also investigated whether the uptake of the SSTR-2-targeting tracers is correlated with pro-inflammatory cytokine and metabolic hormone levels. It was of note that [^{68}Ga]DOTANOC uptake in atherosclerotic plaques positively correlated with plasma IL-6 levels, which can be considered as a marker of systemic inflammation and a pro-inflammatory mediator promoting atherosclerosis [32, 33]. Furthermore, we found a positive trend between [^{68}Ga]DOTANOC and plasma MCP-1 concentration. Although the correlation was not statistically significant, it was biologically rational since MCP-1 is an active mediator of monocyte recruitment during the development of atherosclerosis [2, 34]. It can be speculated that the uptake of [^{68}Ga]DOTANOC in atherosclerotic plaques reflects the abundance of infiltrated macrophages, which is in part governed by secreted MCP-1 levels. Interestingly, plaque [^{68}Ga]DOTANOC uptake associated with plasma leptin and insulin levels, which are known to be often elevated in symptomatic atherosclerosis and to predict coronary events [35–38]. Further studies are still warranted to explore the role of SSTR-2 signaling in the initiation and development of atherosclerosis and to more precisely define whether the uptake of SSTR-2-targeting tracers serves as a true marker of plaque vulnerability.

Finally, we investigated the *in vivo* imaging characteristics of [^{68}Ga]DOTANOC against [^{68}Ga]DOTATATE using head-to-head comparison. Although [^{68}Ga]DOTATATE showed higher plaque-to-wall ratio compared to [^{68}Ga]DOTANOC in *ex vivo* ARG analysis, *in vivo* PET/CT imaging demonstrated that [^{68}Ga]DOTANOC accumulated more in the diseased aorta and had higher target-to-blood ratio in comparison with [^{68}Ga]DOTATATE. These results suggest superior applicability for [^{68}Ga]DOTANOC in the detection of atherosclerotic plaques compared to [^{68}Ga]DOTATATE, but further experiments, employing other atherosclerosis models at different stages of the disease, are still needed to confirm this concept.

Conclusions

We demonstrated that [^{68}Ga]DOTANOC is superior over [^{18}F]FDR-NOC in terms of its feasibility for the detection of macrophage-rich atherosclerotic plaques. [^{68}Ga]DOTANOC accumulated more in atherosclerotic lesions than in pathologically normal vessel areas. These results and characteristics of [^{68}Ga]DOTANOC were similar to or even better than that of [^{68}Ga]DOTATATE, which has previously been shown to be a promising tracer especially for the imaging of coronary atherosclerosis. The present study further strengthens the concept of SSTR-2-based imaging strategy to identify vulnerable plaques in high-risk patients.

Acknowledgments. The authors wish to thank Riikka Siitonen and Aake Honkaniemi for assistance in mouse experiments and Erica Nyman and Sinikka Collanus for technical assistance in tissue sectioning and immunohistochemistry. This study was conducted within the Finnish Center of Excellence in Cardiovascular and Metabolic Diseases supported by the Academy of Finland, the University of Turku, the Turku University Hospital, and the Åbo Akademi University.

Conflict of Interest. The authors declare that they have no conflict of interest.

References

1. Weber C, Noels H (2011) Atherosclerosis: current pathogenesis and therapeutic options. Nat Med 17:1410–1422
2. Hansson GK, Libby P (2006) The immune response in atherosclerosis: a double-edged sword. Nat Rev Immunol 6:508–519
3. Moore KJ, Sheedy FJ, Fisher EA (2013) Macrophages in atherosclerosis: a dynamic balance. Nat Rev Immunol 13:709–721
4. Swirski FK, Nahrendorf M (2013) Leukocyte behavior in atherosclerosis, myocardial infarction, and heart failure. Science 339:161–166
5. Langer HF, Haubner R, Pichler BJ, Gawaz M (2008) Radionuclide imaging: a molecular key to the atherosclerotic plaque. J Am Coll Cardiol 52:1–12
6. Tarkin JM, Joshi FR, Rudd JH (2014) PET imaging of inflammation in atherosclerosis. Nat Rev Cardiol 11:443–457
7. Rudd JH, Narula J, Strauss HW et al (2010) Imaging atherosclerotic plaque inflammation by fluorodeoxyglucose with positron emission tomography: ready for prime time? J Am Coll Cardiol 55:2527–2535
8. Ogawa M, Ishino S, Mukai T et al (2004) ^{18}F-FDG accumulation in atherosclerotic plaques: immunohistochemical and PET imaging study. J Nucl Med 45:1245–1250
9. Zhang Z, Machac J, Helft G et al (2006) Non-invasive imaging of atherosclerotic plaque macrophage in a rabbit model with F-18 FDG PET: a histopathological correlation. BMC Nucl Med 6:3
10. Tahara N, Kai H, Ishibashi M et al (2006) Simvastatin attenuates plaque inflammation: evaluation by fluorodeoxyglucose positron emission tomography. J Am Coll Cardiol 48:1825–1831
11. Aziz K, Berger K, Claycombe K et al (2008) Noninvasive detection and localization of vulnerable plaque and arterial thrombosis with computed tomography angiography/positron emission tomography. Circulation 117:2061–2070
12. Paulmier B, Duet M, Khayat R et al (2008) Arterial wall uptake of fluorodeoxyglucose on PET imaging in stable cancer disease patients indicates higher risk for cardiovascular events. J Nucl Cardiol 15:209–217
13. Buettner C, Rudd JH, Fayad ZA (2011) Determinants of FDG uptake in atherosclerosis. JACC Cardiovasc Imaging 4:1302–1304
14. Rominger A, Saam T, Vogl E et al (2010) *In vivo* imaging of macrophage activity in the coronary arteries using ^{68}Ga-DOTATATE PET/CT: correlation with coronary calcium burden and risk factors. J Nucl Med 51:193–197
15. Li X, Bauer W, Kreissl MC et al (2013) Specific somatostatin receptor II expression in arterial plaque: ^{68}Ga-DOTATATE autoradiographic, immunohistochemical and flow cytometric studies in apoE-deficient mice. Atherosclerosis 230:33–39
16. Li X, Samnick S, Lapa C et al (2012) ^{68}Ga-DOTATATE PET/CT for the detection of inflammation of large arteries: correlation with ^{18}F-FDG, calcium burden and risk factors. EJNMMI Res 2:52
17. Wild D, Mäcke HR, Waser B et al (2005) ^{68}Ga-DOTANOC: a first compound for PET imaging with high affinity for somatostatin receptor subtypes 2 and 5. Eur J Nucl Med Mol Imaging 32:724
18. Wild D, Schmitt JS, Ginj M et al (2003) DOTA-NOC, a high-affinity ligand of somatostatin receptor subtypes 2, 3 and 5 for labelling with various radiometals. Eur J Nucl Med Mol Imaging 30:1338–1347
19. Kiviniemi A, Gardberg M, Autio A et al (2014) Feasibility of experimental BT4C glioma models for somatostatin receptor 2-targeted therapies. Acta Oncol 53:1125–1134
20. Heinonen SE, Leppänen P, Kholová I et al (2007) Increased atherosclerotic lesion calcification in a novel mouse model combining insulin resistance, hyperglycemia, and hypercholesterolemia. Circ Res 101:1058–1067
21. Silvola JM, Saraste A, Laitinen I et al (2011) Effects of age, diet, and type 2 diabetes on the development and FDG uptake of atherosclerotic plaques. JACC Cardiovasc Imaging 4:1294–1301
22. Körner M, Waser B, Schonbrunn A et al (2012) Somatostatin receptor subtype 2A immunohistochemistry using a new monoclonal antibody selects tumors suitable for *in vivo* somatostatin receptor targeting. Am J Surg Pathol 36:242–252
23. Belosi F, Cicoria G, Lodi F et al (2013) Generator breakthrough and radionuclidic purification in automated synthesis of ^{68}Ga-DOTANOC. Curr Radiopharm 6:72–77
24. Li XG, Autio A, Ahtinen H et al (2013) Translating the concept of peptide labeling with 5-deoxy-5-[^{18}F]fluororibose into preclinical practice: ^{18}F-labeling of Siglec-9 peptide for PET imaging of inflammation. Chem Commun (Camb) 49:3682–3684
25. Li XG, Helariutta K, Roivainen A et al (2014) Using 5-deoxy-5-[^{18}F]fluororibose to glycosylate peptides for positron emission tomography. Nat Protoc 9:138–145
26. Rinne P, Silvola JM, Hellberg S et al (2014) Pharmacological activation of the melanocortin system limits plaque inflammation and ameliorates vascular dysfunction in atherosclerotic mice. Arterioscler Thromb Vasc Biol 34:1346–1354
27. Silvola JM, Laitinen I, Sipilä HJ et al (2011) Uptake of ^{68}gallium in atherosclerotic plaques in LDLR$^{-/-}$ApoB$^{100/100}$ mice. EJNMMI Res 1:14
28. Patel YC (1999) Somatostatin and its receptor family. Front Neuroendocrinol 20:157–198
29. Adams RL, Adams IP, Lindow SW et al (2005) Somatostatin receptors 2 and 5 are preferentially expressed in proliferating endothelium. Br J Cancer 92:1493–1498
30. Armani C, Catalani E, Balbarini A et al (2007) Expression, pharmacology, and functional role of somatostatin receptor subtypes 1 and 2 in human macrophages. J Leukoc Biol 81:845–855
31. Schatka I, Wollenweber T, Haense C et al (2013) Peptide receptor-targeted radionuclide therapy alters inflammation in atherosclerotic plaques. J Am Coll Cardiol 62:2344–2345
32. Yudkin JS, Kumari M, Humphries SE, Mohamed-Ali V (2000) Inflammation, obesity, stress and coronary heart disease: is interleukin-6 the link? Atherosclerosis 148:209–214
33. Schuett H, Oestreich R, Waetzig GH et al (2012) Transsignaling of interleukin-6 crucially contributes to atherosclerosis in mice. Arterioscler Thromb Vasc Biol 32:281–290
34. Sheikine Y, Hansson GK (2004) Chemokines and atherosclerosis. Ann Med 36:98–118
35. Wallace AM, McMahon AD, Packard CJ et al (2001) Plasma leptin and the risk of cardiovascular disease in the west of Scotland coronary prevention study (WOSCOPS). Circulation 104:3052–3056
36. Koh KK, Park SM, Quon MJ (2008) Leptin and cardiovascular disease: response to therapeutic interventions. Circulation 117:3238–3249
37. Ducimetiere P, Eschwege E, Papoz L et al (1980) Relationship of plasma insulin levels to the incidence of myocardial infarction and coronary heart disease mortality in a middle-aged population. Diabetologia 19:205–210
38. Stout RW (1990) Insulin and atheroma. 20-yr perspective. Diabetes Care 13:631–654